An Impact of Subgrid-Scale Ice–Ocean Dynamics on Sea-Ice Cover

DAVID M. HOLLAND

Courant Institute of Mathematical Sciences, New York, New York

(Manuscript received 4 March 2000, in final form 2 August 2000)

ABSTRACT

A coupled sea-ice–ocean numerical model is used to study the impact of an ill-resolved subgrid-scale sea-ice–ocean dynamical process on the areal coverage of the sea-ice field. The process of interest is the transmission of stress from the ocean into the sea-ice cover and its subsequent interaction with the sea-ice internal stress field. An idealized experiment is performed to highlight the difference in evolution of the sea-ice cover in the circumstance of a relatively coarse-resolution grid versus that of a fine-resolution one. The experiment shows that the ubiquitous presence of instabilities in the near-surface ocean flow field as seen on a fine-resolution grid effectively leads to a *sink* of sea-ice areal coverage that does not occur when such flow instabilities are absent, as on a coarse-resolution grid. This result also implies that a fine-resolution grid may have a more efficient atmosphere–sea-ice–ocean thermodynamic exchange than a coarse one. This sink of sea-ice areal coverage arises because the sea-ice undergoes sporadic, irreversible plastic failure on a fine-resolution grid that, by contrast, does not occur on a coarse-resolution grid. This demonstrates yet again that coarse-resolution coupled climate models are not reaching fine enough resolution in the polar regions of the world ocean to claim that their numerical solutions have reached convergence.

1. Introduction

Numerous observational and modeling studies carried out over the last few decades, investigating a wide variety of aspects of the physical environment of the polar regions, have shown increasing evidence that the polar regions likely play an important role in the overall regulation of the climatic state of planet Earth. These cold places act in large part as the heat sink region for the global atmosphere and ocean and thereby serve to balance the heat source regions of the lower latitudes. In this manner the polar regions help maintain the basic thermodynamic balance of our climate system. Understanding the variability in this physical environment, either of natural origin or anthropogenically influenced, is an important goal and at the same time an elusive one as the complexity of the physical environment, and the numerous feedback processes operating between various components, make this a challenging scientific problem. Recently, with the ever-increasing observational database, we are beginning to see definite signs of significant variability in this system, and as of yet we unfortunately do not understand the fundamental reasons for such variability.

The variability that we are seeing is showing up in most all components that make up the physical environment of the polar regions. In the Arctic, the observed variability of the stratospheric polar vortex has been implicated in some of the interannual and secular variability of the surface winds and temperatures (Thompson and Wallace 1998). This phenomenon, known as the Arctic Oscillation, may have effects more far reaching than just in the atmosphere as, for example, a weakening of the wind-driven Beaufort Gyre could further reduce the extent and thickness of the Arctic pack ice. The sea ice itself, in the Arctic, has been the center of much attention, particularly since it has recently been revealed from submarine sea-ice draft data that approximately forty percent of the average thickness has been depleted in the last few decades (Rothrock et al. 1999). The waters of the Arctic Ocean have also been undergoing variability as the cold halocline, which serves to insulate the sea-ice cover from the large heat reservoir of the deeper Atlantic layer waters, has been retreating in areal extent (Steele and Boyd 1998). In the Antarctic, there has also been evidence of variability, with recent observations indicating eastward-propagating anomalies in the sea level pressure, sea-ice extent, and sea surface temperature fields. This phenomenon, known as the Antarctic Circumpolar Wave, dominates the interannual climate variability signal in this region (White and Peterson 1996). Aside from observational studies, modeling efforts also point to variability occurring in the polar regions that has global impacts. In the particular context of the modeling of various global warming

Corresponding author address: Dr. David M. Holland, Courant Institute of Mathematical Sciences, New York University, 251 Mercer Street, New York, NY 10012-1185.
E-mail: holland@cims.nyu.edu

scenarios, a polar amplification of the warming pattern, partly due to the feedback process between the sea-ice cover and the effective surface albedo, is seen (for a review of relevant modeling studies see Climate Research Committee 1995).

While these observational and modeling studies provide some evidence of the variability and even possible instability of some aspects of the polar environments, particularly in the case of the relatively tenuous existence of the sea-ice cover, our knowledge of this harsh environment is far from complete. We need to carry out observation and modeling studies so that we can obtain a solid understanding of the physical mechanisms that control the variability of the polar regions and a deeper insight into their importance to the global climate system. In particular, with regards to modeling activities, which are the focus of this study, making concrete advances requires improvements in, among other things, the description of all relevant physical processes and in the speed of computational platforms. The present situation with respect to the state-of-the-art global climate models is that some physical processes are absent from the models and, with the rather coarse-resolution grids used, some physical processes are ill resolved. In other words, these present-day models may be deficient in at least two ways: one is that some key physical processes may not yet have been included in the mathematical framework of the computer codes and the second is that such processes, while apparently present are in fact not resolvable by the rather coarse grids and are therefore in practical terms missing from the simulations. This naturally leads us to question whether the simulations obtained from such models are in fact physically meaningful.

Consider but one example of this, what are the implications of a coarse-grid resolution in the specific context of modeling the interaction between the ocean surface and lower atmosphere in the polar regions where a sea-ice cover acts as intermediary between the ocean and atmosphere? From satellite observations we are beginning to see that mesoscale ocean eddies do have an imprint directly upon the visible appearance of the sea-ice cover (see Fig. 1). A coarse-resolution model does not resolve the ocean eddy field and by inference it does not simulate the impacts of the ocean eddy field upon the sea-ice cover. In the present work we will show that resolving this ocean eddy field may be of some consequence in producing additional lead area in the sea-ice cover and thus likely impacting the efficiency of atmosphere–ocean heat and freshwater exchange. In general, the ability of models to resolve the ocean eddy field in polar regions is made all the more difficult by the fact that the horizontal scale of ocean eddy fluctuations, that is, the internal Rossby radius of deformation decreases with increasing latitude. If a model lacks sufficient resolution it will not be able to simulate the impacts of the development of geostrophic turbulence or other ocean flow-related instabilities on the evolution of the climate system. This deficiency being an artifact of nothing other than the coarseness of the resolution of the underlying grid used in the numerical simulation. The main purpose of this study is to investigate how such a misrepresentation of the near-surface ocean eddy field might impact the simulation of the sea-ice cover in a global climate model.

It is not a straightforward task to determine whether an important physical process is missing or, equally unsatisfactory, is ill resolved in a climate simulation. It is often all the more onerous a task to make corrections for such deficiencies. A standard remedy for such deficiencies that has grown up in the modern computational fluid dynamics paradigm is that of formulating subgrid-scale (SGS) representations, or parameterizations, of the missing or ill-resolved physical processes. The most widespread SGS parameterization currently in use is that describing the viscous dissipation of energy and momentum at the smallest possible scales of fluid motion. In fact, producing an accurate parameterization of such viscous processes is still an active area of research in the more general field of fluid dynamics. Part of the difficulty associated with the realization of a meaningful parameterization lies in the development of numerical schemes that ensure conservation of basic quantities such as mass, momentum, and kinetic energy, as otherwise it is difficult, if not impossible, to separate the explicit effects of the parameterization on a simulation from those of a hidden, numerical origin. In geophysical fluid dynamics, SGS parameterizations are also quite widespread, as in, for example, atmospheric general circulation modeling where it is commonplace to invoke an orographic gravity wave drag parameterization (McFarlane 1987) to capture the ill-resolved effects of orography on the atmospheric momentum balance as caused by internal wave breaking events. In ocean general circulation modeling, as for example in those employing height as the independent vertical coordinate axis, it is desirable to parameterize the impacts of the ill-resolved along-isopycnal eddy mixing of dynamic tracers by using a mixing-velocity parameterization (Gent and McWilliams 1990). One ancillary objective of the present study is to begin to question how the effects of the ill-resolved ocean eddy field upon the sea-ice cover might eventually be represented by a suitable physically based parameterization.

With regards to sea-ice modeling, attention has been paid to SGS parameterizations but that attention has not been concerned, as is the case in the present study, with the effects of the near-surface ocean eddy field upon the sea-ice cover. We now mention three SGS parameterizations in use in sea-ice modeling and note that these parameterizations are all ultimately a direct consequence of the spatial inhomogeneity of a sea-ice-covered ocean on the horizontal scale of a typical climate model grid cell. The first SGS parameterization developed in this context arose from the realization that the sea-ice thickness varies greatly over a typical grid cell scale. This

FIG. 1. RADARSAT standard beam image of a small section of the Weddell Sea northward and adjacent to the Dronning Maud Land. The image is an approximately 100 km by 100 km square and was taken during yearday 122 of 1999. The image is superimposed on a larger solid black square. The edges of that black square provide orientation of the image with respect to the earth's lines of latitude (i.e., along vertical edges of the square) and longitude (i.e., along horizontal edges of the square). The bright white area occupying the southernmost portion of the RADARSAT image is glacial ice originating from the Antarctic ice sheet. The other, less bright white areas of the image show the sea-ice cover while the darkest areas show the surface of the ocean with little fractional sea-ice cover. The signature of the near-surface ocean eddy field in the sea-ice concentration field is evident from the various swirling patterns seen in the image. (The image was provided courtesy of M. Drinkwater, JPL, ADRO Project 164.)

realization has given rise to the implementation of sea-ice thickness distributions whereby the different thickness categories of the sea ice are individually evolved within a grid cell (Thorndike et al. 1975; Hibler 1980). In such models the sea-ice compressive strength is also SGS dependent in that it is formulated with reference to potential energy changes associated with ridging events. One reason that it is important to attempt to individually quantify the various thickness classes contained within a given grid cell is that the thermodynamic and dynamic fluxes through the sea-ice cover are both critically dependent on the thickness of the sea ice. Particularly sensitive in this context is the accurate computation of the areal fraction of the thin sea-ice cover because of its ability to transmit far greater heat fluxes than that of the relatively inert, thicker sea-ice-covered part of the ocean surface.

A second common SGS parameterization to arise in sea-ice modeling studies involves estimating the areally averaged fluxes between the lower atmosphere and the sea ice. From the point of view of making an accurate computation of the various fluxes at the lower boundary of the atmosphere over a sea-ice-covered ocean, the spatial inhomogeneity of the surface conditions at a sufficiently large scale would allow justification for simple parameterization schemes of surface fluxes based on boundary layer similarity theory. With the actual case being that surface inhomogeneity occurs at scales *smaller* than that resolvable by the numerical grid, the usual SGS parameterization of surface fluxes is then no longer applicable. In this case it is necessary to consider grid-cell averages of the surface fluxes of heat, freshwater, and momentum. The realization of this has, in part, led to the development of the concept of a ''blending

height'' so as to derive the correct areally averaged surface fluxes of heat and momentum (Claussen 1991). The blending-height concept has been successfully applied in large-scale coarse-resolution modeling of sea-ice momentum exchange (Stossel and Claussen 1993) and thermodynamic exchange (Grotzner et al. 1996) over a heterogeneous sea-ice cover.

A third SGS sea-ice effect concerns the manner in which salt fluxes, arising from sea-ice growth, are distributed to the near-surface ocean waters, the details of which can have important ramifications on the overall evolution of the sea-ice and ocean states in a coarse-resolution model (Duffy and Caldeira 1999). The key point is to question how to treat the upper-ocean vertical mixing process that is forced by an imposed surface buoyancy flux having an inherently SGS nature. It has been found that treating the surface fluxes such that they affect only a small fraction of a grid cell produces superior simulation results, when compared to observations, to the approach whereby the fluxes are uniformly distributed over an entire coarse-resolution grid cell.

In this study we look at a new SGS sea-ice–ocean phenomenon relating to the presence of a mesoscale ocean eddy field. This phenomenon, and its treatment in terms of a SGS parameterization, has not been addressed in previous sea-ice SGS parameterization studies and that fact motivates the present study. The outline of the remainder of this paper is as follows. In section 2, we present the fundamental equations upon which the coupled sea-ice–ocean numerical model is based. In section 3, the results of application of the coupled model in an idealized, doubly periodic box-domain configuration are reported. The emphasis is on showing that SGS phenomenon, related to the occurrence of ocean geostrophic turbulence can impact the evolution of the sea-ice cover and thus, by implication, the vertical exchange of fluxes between the atmosphere and ocean. Conclusions drawn from this idealized study are presented in section 4 as well as a discussion of their relevance to present-day global climate modeling efforts.

2. Model description

As part of a longer-term climate modeling development strategy, which has as its main objective the investigation of various aspects of the climate of the polar regions, a new coupled numerical modeling system is being constructed named the Polar Ocean Land Atmosphere and Ice Regional (POLAIR) model. We now present the detailed conservation equations of the coupled sea-ice–ocean components of this model. The other model components, most notably the atmosphere, will be integrated within this modeling framework in future studies. The main components of the present system are an isopycnic-coordinate ocean model (Bleck 1998) and a dynamic-thermodynamic sea-ice model. As part of the overall strategy in coupling a sea-ice model to an isopycnic-ocean model, it is necessary, for completeness, to introduce two additional models. The first is a viscous-sublayer model at the sea-ice–ocean interface to handle the details of the thermodynamic interaction of the base of the sea ice with the mixed layer waters of the ocean (Holland and Jenkins 1999). The second is a turbulent mixed layer model to guide the interaction of the mixed layer waters with the interior isopycnic ocean waters (Gaspar 1988). Consequently, there are actually four component submodels making up the overall coupled model and additionally there are idealized atmospheric forcing fields to consider. In the equations that follow, a subscript of *a, i, s, m,* or *o* refers to a variable of the atmosphere, sea-ice, viscous-sublayer, mixed layer, and isopycnic-ocean model components, respectively. A doubly subscripted variable generally refers to a quantity at the physical interface between two component submodels.

a. Ocean model

The primitive equation isopycnic coordinate ocean model used is a modified version of the Miami Isopycnic Coordinate Ocean Model (MICOM) developed at the University of Miami (Bleck and Smith 1990). It has four main prognostic equations: one equation for the horizontal velocity vector, a mass continuity or equivalently a layer thickness tendency equation, and two conservation equations for the buoyancy-related variables (i.e., potential temperature and salinity):

$$\frac{\partial \mathbf{v}_o}{\partial t} + \boldsymbol{\nabla}\frac{\mathbf{v}_o^2}{2} + (f + \zeta_o)\hat{\mathbf{k}} \times \mathbf{v}_o + \boldsymbol{\nabla} M_o = \frac{g}{h_o}(\boldsymbol{\tau}_{oo}^{-} - \boldsymbol{\tau}_{oo}^{+}) + \frac{1}{h_o}\boldsymbol{\nabla} \cdot (\kappa_o^v h_o \boldsymbol{\nabla} \mathbf{v}_o) \tag{2.1}$$

$$\frac{\partial h_o}{\partial t} + \boldsymbol{\nabla} \cdot (\mathbf{v}_o h_o) = \boldsymbol{\nabla} \cdot (\kappa_o^h \boldsymbol{\nabla} h_o) \tag{2.2}$$

$$\frac{\partial (h_o C_o)}{\partial t} + \boldsymbol{\nabla} \cdot (\mathbf{v}_o h_o C_o) = \boldsymbol{\nabla} \cdot (\kappa_o^C h_o \boldsymbol{\nabla} C_o) + \Im_o^C. \tag{2.3}$$

In these relations $\mathbf{v}_o = (u_o, v_o)$ is the horizontal ocean velocity vector, f the Coriolis parameter (spatially varying), $\zeta_o = \partial v_o/\partial x - \partial u_o/\partial y$ the relative vorticity, $\hat{\mathbf{k}}$ the vertical unit vector, $M_o = \alpha_o^\theta p_o + \phi_o$ the Montgomery potential, α_o^θ the potential specific volume, p_o the pressure, $\phi_o = gz$ the geopotential, g the gravitational acceleration, $\boldsymbol{\tau}_{oo}^{\pm}$ the shear stress at a layer interface (with superscript ''$-$'' referring to the upper interface of a layer and ''$+$'' the lower), h_o the thickness of a layer (in pressure units), κ_o^v the isopycnic eddy viscosity, κ_o^h and κ_o^C the diffusivities, C_o represents either one of the model's active thermodynamic variables (i.e., potential temperature θ_o or salinity S_o) as well as arbitrary passive tracers, and $\Im_o^C$ represents the sum of all forcings on the

TABLE 1. Interfacial stresses and drag coefficients.

Parameter	Symbol	Units	Value
Air drag coefficient to ocean surface	c_{oa}	dimensionless	1.5×10^{-3}
Air frictional stress to ocean surface	$\boldsymbol{\tau}_{oa}$	Pa	
Air drag coefficient to sea-ice surface	c_{ia}	dimensionless	3.00×10^{-3}
Air frictional stress to sea-ice surface	$\boldsymbol{\tau}_{ia}$	Pa	
Ocean drag coefficient of internal interfaces	c_{oo}	dimensionless	1.00×10^{-5}
Ocean frictional stress at interior interfaces	$\boldsymbol{\tau}_{oo}$	Pa	
Ocean drag coefficient at ocean bottom	c_{bo}	dimensionless	2.50×10^{-3}
Ocean frictional stress at ocean bottom	$\boldsymbol{\tau}_{bo}$	Pa	
Sea-ice drag coefficient to ocean surface	c_{oi}	dimensionless	3.00×10^{-3}
Sea-ice frictional stress to ocean surface	$\boldsymbol{\tau}_{oi}$	Pa	

tracer variable C_o. The independent variables x, y, and t have their usual meanings.

As these equations are derived under the hydrostatic and Boussinesq approximations, the vertical component of the momentum balance is a diagnostic equation, which in the isopycnic framework takes on the form:

$$\frac{\partial M_o}{\partial \alpha_o^\theta} = p_o. \tag{2.4}$$

The ocean conservation equations, as well as the analogous sea-ice equations presented later, are spatially discretized on the Arakawa C grid (Arakawa and Lamb 1977) and temporally integrated forward using leapfrog stepping with filtering (Asselin 1972). The equation of state utilized to compute potential density ρ_o^θ, and its inverse the potential specific volume α_o^θ, is an approximation of the United Nations Educational, Scientific and Cultural Organization equation of state (Millero et al. 1980) in the form of a polynomial that is cubic in potential temperature, quadratic in pressure, and linear in salinity (Brydon et al. 1999).

There are a variety of horizontal interfaces of like and dislike fluids, or fluids and solids, occurring within the model domain. These interfaces occur between the atmosphere and ocean mixed layer, the atmosphere and sea ice, the sea ice and ocean mixed layer, the ocean isopycnic interior layers themselves, and the bottom most isopycnic layer and the sea floor. The various interfacial stresses relating to the ocean model, as applied to the momentum equation (2.1), are formulated as quadratic drag laws of the form:

$$\boldsymbol{\tau}_{oa} = \rho_a^r c_{oa} |\mathbf{v}_a - \mathbf{v}_o| (\mathbf{v}_a - \mathbf{v}_o) \qquad \boldsymbol{\tau}_{oo} = \rho_o^r c_{oo} |\Delta \mathbf{v}_o| \Delta \mathbf{v}_o$$
$$\boldsymbol{\tau}_{bo} = \rho_o^r c_{bo} |\mathbf{v}_o| \mathbf{v}_o, \tag{2.5}$$

where ρ_a^r and ρ_o^r are reference densities for the atmosphere and ocean, respectively. The three stresses defined represent that between the air and the ocean $\boldsymbol{\tau}_{oa}$, between the ocean layers $\boldsymbol{\tau}_{oo}$ themselves, and between the bottom most ocean layer and the sea floor $\boldsymbol{\tau}_{bo}$. The values of the various empirical drag coefficients c_{oa}, c_{oo}, and c_{bo}, are given in Table 1. The velocity of an ocean layer has already been defined as $\mathbf{v}_o$, and accordingly the velocity jump occurring at the interface between two adjacent layers is defined as $\Delta \mathbf{v}_o$. The wind velocity is denoted $\mathbf{v}_a$.

In order to accommodate strong buoyancy forcing at its surface, a common characteristic of an isopycnic model is that it treats its topmost layer as nonisopycnic. Such a layer is referred to as a mixed layer and sits atop the pure isopycnic ''interior'' layers. The mixed layer serves as the interface between the adiabatic ocean interior and the ocean surface density fluxes that arrive via buoyancy inputs from the atmosphere (and in the polar context of this study, also from the sea ice). While all model layers adhere to the continuity equation (2.2), the thickness of the mixed layer is unique in that it is also influenced by a turbulent kinetic energy (TKE) balance of surface frictional stress, surface buoyancy input, and a parameterization of dissipative processes (Gaspar 1988). To write down a conservation equation for TKE, we first need define the buoyancy b_o in a layer as

$$b_o = -g \frac{(\rho_o^\theta - \rho_o^r)}{\rho_o^r}. \tag{2.6}$$

The rate of entrainment of fluid w_m across the basal interface of the mixed layer is then calculable from the following TKE budget equation:

$$\frac{\Delta b_o w_m}{2} = \frac{c_m (u_{oi}^*)^3}{h_m} + \frac{B_m}{2} - \varepsilon_m, \tag{2.7}$$

where Δb_o is the layerwise jump in buoyancy across the mixed layer base, c_m an empirical constant, u_{oi}^* the friction velocity at the sea-ice–ocean interface, B_m the buoyancy flux due to surface forcing, h_m the thickness of the mixed layer, and ε_m the parameterized dissipation of TKE (see Gaspar 1988 for further details).

b. Sea-ice model

The sea-ice model includes descriptions of both dynamical and thermodynamical processes. The statement of momentum conservation involves a description of advective, rotational, and dissipative terms as used for the ocean model layers described earlier but now with a special treatment of ice–ice interaction via a cavitating-fluid rheology (Flato and Hibler 1992). The sea-ice thickness and concentration fields are determined by

considering the divergence of heat and freshwater fluxes at the various sea-ice-related interfaces with special attention paid to the sea-ice–ocean interface where a viscous-sublayer parameterization is employed (Holland and Jenkins 1999).

As one writes down the formulation of the dynamical and thermodynamical equations for sea ice and then compares to those used earlier for an isopycnic ocean layer then the obvious similarities lead to the observation that, with small modification, the ocean equations (2.1)–(2.3) can be used as a basis for a mathematical description of the sea ice. In this sense, we treat sea ice as just another ''isopycnic'' layer of fluid, but having different internal stress properties—the sea ice is obviously not a Newtonian fluid as is the case for seawater. The benefit to be gained from such an approach is an economical one in that almost exactly the same computer code may be used for both the ocean and sea ice. This furthermore implies that a consistent numerical scheme can be used to solve both the isopycnic ocean and sea-ice equations, with exceptions to this approach being noted in the discussion below. The sea-ice equations are then

$$\frac{\partial \mathbf{v}_i}{\partial t} + \boldsymbol{\nabla}\frac{\mathbf{v}_i^2}{2} + (f + \xi_i)\hat{\mathbf{k}} \times \mathbf{v}_i + \boldsymbol{\nabla} M_i = \frac{(\boldsymbol{\tau}_{ia} - \boldsymbol{\tau}_{oi})}{\rho_i h_i} + \frac{1}{h_i}\boldsymbol{\nabla} \cdot (\kappa_i^v h_i \boldsymbol{\nabla}\mathbf{v}_i) \tag{2.8}$$

$$\frac{\partial h_i}{\partial t} + \boldsymbol{\nabla} \cdot (\mathbf{v}_i h_i) = \boldsymbol{\nabla} \cdot (\kappa_i^h \boldsymbol{\nabla} h_i) + \Im_i^h \tag{2.9}$$

$$\frac{\partial C_i}{\partial t} + \boldsymbol{\nabla} \cdot (\mathbf{v}_i C_i) = \boldsymbol{\nabla} \cdot (\kappa_i^C \boldsymbol{\nabla} C_i) + \Im_i^C. \tag{2.10}$$

In these relations $\mathbf{v}_i = (u_i, v_i)$ is the horizontal velocity vector, $\zeta_i = \partial v_i/\partial x - \partial u_i/\partial y$ the relative vorticity, $M_i = \alpha_i p_i + \phi_i$ the Montgomery potential, α_i the specific volume, p_i the pressure, $\phi_i = g\eta_o$ the geopotential, η_o the sea surface elevation with respect to a fixed geoid, $\boldsymbol{\tau}_{ia}$ the wind induced sea-ice surface shear stress vector, $\boldsymbol{\tau}_{oi}$ the analogous sea-ice bottom-drag stress vector, h_i the thickness (in meters units), κ_i^v the eddy viscosity, κ_i^h and κ_i^C the eddy diffusivities, C_i the concentration, and $\Im_i^h$ and $\Im_i^C$ represent the sum of all thermodynamic forcings on the sea-ice thickness and concentration fields, respectively. It should be noted that whereas the isopycnic ocean equations conventionally treat the ocean thickness h_o with measurement units of Pascals the sea-ice thickness h_i is expressed in units of meters. The sea-ice concentration C_i is defined as the fraction of a grid cell covered by sea ice and is bounded between zero and unity. As a convenience, we define the areal fraction of leads (i.e., open water) in a grid cell as $\tilde{C}_i = 1 - C_i$.

The description of sea ice embodied by the cavitating-fluid rheology is that of a fluid having no resistance to a divergent stress but a finite resistance to a convergent stress. Generally, lateral shear stresses are not considered. As the sea ice is pulled apart by horizontal interfacial stresses, by nonlinear accelerations, or by rotational forces, there are no compensatory internal stresses present that can retard such divergent motion and consequently leads can thus appear in the sea-ice cover. In response to such divergent motion the sea-ice concentration C_i may locally lower its value. By contrast, as sea ice converges, again for whatever the dynamical reason, some resistive stress can be experienced by the sea-ice floes, the amount of which depends on the local plastic strength of the sea-ice pack.

This plastic strength is parameterized based on an empirical dependence that relates sea-ice thickness and concentration to strength (Hibler 1979). This parameterization may be equivalently stated in terms of a sea-ice Montgomery potential that has a limiting value according to

$$M_i^{\max} = \alpha_i p_i^* h_i e^{-k_i^* \tilde{C}_i}. \tag{2.11}$$

The parameterization makes use of the empirical constants p_i^* and k_i^* that have values of 27.5×10^3 kN m^{-2} and 20 (nondimensional), respectively (Hibler 1979). This formulation has a linear dependence on the sea-ice thickness. As an alternative empirical parameterization, and particularly so for thinner categories of sea ice, it has been suggested that a quadratic dependence on the sea-ice thickness may be more appropriate (Overland and Pease 1988):

$$M_i^{\max} = \alpha_i p_i^* h_i^2 e^{-k_i^* \tilde{C}_i}, \tag{2.12}$$

where the empirical constant p_i^* assumes a modified value of 1.45×10^3 kN m^{-3} and k_i^* retains its earlier value. We shall use this latter formulation in the present study, as we are particularly interested in the behavior of a relatively thin sea-ice cover.

The usual strategy in implementing the cavitating-fluid rheology is to begin with a so-called ''free-drift'' solution in which the rheological stresses are ignored and the sea-ice velocity field is determined by a balance of the Coriolis force and the atmosphere—sea-ice and sea-ice–ocean frictional stresses. Subsequently, an iterative procedure is performed to correct the sea-ice velocity field to bring it into agreement with the iteratively developing rheological stresses. The key point is that under divergent flow conditions the sea-ice pressure field is effectively zero and the rheology has no impact on the flow regime; under converging flow conditions the sea-ice pressure, which can only rise to its maximum, failure-limited value can greatly affect the flow regime. During flow convergence, if the computed pressure field is below its failure-limited value then sea-ice convergence is forced to zero and the sea-ice field acts

essentially as a horizontally rigid medium. Should the sea-ice pressure rise above the maximum, failure-limited value then plastic flow ensues with convergence of sea-ice mass into a grid cell (Flato and Hibler 1992).

The frictional stresses applied to the sea-ice momentum equation (2.8) are taken to be quadratic in form, as for the analogous ocean stresses (2.5). A horizontal rotational angle is not applied to the stress vector defined between either the flow of the sea ice and ocean or the sea ice and atmosphere. As the ocean currents utilized in the stress calculations are taken from the ocean mixed layer, and are not the geostrophic currents from the oceanic interior, it would be inappropriate to apply a rotational angle. The mixed layer currents $\mathbf{v}_m$ computed from the ocean model already have the Ekman-related turning angle accounted for in their flow vector directions. As regards the atmospheric winds $\mathbf{v}_a$, when employed in the current coupled model scheme they are input to the model as either idealized wind patterns or are winds taken from an observational database. For idealized winds a rotational angle is not meaningful while for winds from an observational database a rotational angle may be appropriate depending on the details of how those winds were originally created. The formulation of the frictional stress on the sea-ice surface and underside is then represented as

$$\boldsymbol{\tau}_{ia} = \rho_a^r c_{ia} |\mathbf{v}_a - \mathbf{v}_i| (\mathbf{v}_a - \mathbf{v}_i)$$
$$\boldsymbol{\tau}_{oi} = \rho_o^r c_{oi} |\mathbf{v}_i - \mathbf{v}_o| (\mathbf{v}_i - \mathbf{v}_o), \qquad (2.13)$$

where c_{ia} and c_{oi} are the respective empirical drag coefficients for sea-ice–atmosphere and sea-ice–ocean frictional momentum exchange. Their numerical values are provided in Table 1.

The thermodynamic growth of sea-ice thickness h_i and the concomitant increase in sea-ice areal concentration C_i are modeled by the source terms $\Im_i^h$ and $\Im_i^C$, respectively. As the focus of the current study is on sea-ice dynamics, and not thermodynamics, the interested reader is referred to earlier literature for a detailed discussion of the treatment of these terms (Holland et al. 1993; Holland 1998; Holland and Jenkins 1999).

3. Numerical experiment

In this section we look at the response of the sea-ice–ocean system using a fine-resolution numerical model that explicitly resolves the near-surface ocean eddy field. The modeling strategy is to continually populate the near-surface ocean with a field of random eddies, which under the dynamical constraint of planetary rotation, will produce a flow having features resembling that of geostrophic turbulence. We then want to observe how the generated near-surface ocean eddies interact with the sea-ice cover. This experiment sets the stage for an implicit comparison of such an ocean eddy-resolving simulation to the situation whereby the resolution is coarse and ocean eddies are not resolved. Such a comparison will help answer the question as to the overall importance of resolving the near-surface ocean eddy field in a sea-ice–ocean coupled model simulation. First though, we describe details of the experiment configuration.

a. Model configuration

The model simulations are performed in a domain configured as an idealized square box with side lengths of 100 km. The model grid is a regular projection so that all grid boxes are square with a width of approximately 1 km. The model domain spans 103 grid points west–east and similarly south–north. The domain is doubly periodic and thus there are no solid sidewalls along any lateral edge. The sea-ice and oceanic flows are thus reentrant at the eastern and western boundaries, and similarly at the southern and northern boundaries. Under the constraint of this relatively fine-resolution grid spacing, the model equations are stepped forward in time using a split-explicit technique with the slower-moving baroclinic flow stepped at 75 s and the faster-moving barotropic at 2.5 s. The Coriolis parameter f is set to a constant value of -1.4×10^{-4} s^{-1} as representative of its value in the Southern Ocean. The actual variation of Coriolis parameter with latitude is not significant given the limited latitudinal extent of the model domain.

In the vertical coordinate direction the ocean model consists of two layers. The top layer being a 100-m-thick mixed layer and the bottom layer representing the interior ocean, wholly as a single layer. This latter simplification is justified as we are focusing primarily on the interaction of the ocean mixed layer with an overlying layer of sea ice. The details of flow in the ocean interior, away from the mixed layer, being necessarily of lesser consequence in the present context. Consistent with this simplifying approach the sea-floor topography is everywhere flat. As an initial condition, the ocean isopycnals are set to be horizontally flat with the vertical temperature and salinity profiles, both horizontally homogeneous, set according to an idealization suitable for the polar region. The idealization is taken from a hydrographic atlas of the Southern Ocean (Olbers et al. 1992) based on numerous observations. The water column thus described is relatively weak in stratification by global ocean standards.

An induced ocean eddy field is the only energy source generating fluid motion in the model domain as there are neither mean background ocean currents nor atmospheric winds. The ocean eddy field is created by adding a small random velocity component to each ocean model velocity grid point at each model time step. As the ocean model integrates forward in time it organizes these random perturbations into an overall field of geostrophic ocean eddies. These ocean eddies are constantly growing in strength due to the addition of the small random velocity component; at the same time they are constantly decaying in strength due to the lateral

viscosity of the ocean model. This viscosity is parameterized to be proportional to the deformation of the ocean flow field (Smagorinsky 1963). In this manner we create and maintain a geostrophic, turbulent eddy flow in the mixed layer having peak flow velocities of order 50 cm s^{-1}, consistent with the more energetically observed eddies in the real ocean.

With particular reference to the Weddell Sea of the Southern Ocean, where the mean ocean flow field is relatively small having a magnitude of just a few centimeters per second, observations show that larger, fluctuating currents of order tens of centimeters per second occur in the near-surface waters and especially in the near-coastal zone (Fahrbach et al. 1994). The physical mechanism responsible for the origin of these observed, large fluctuations in the near-surface currents has not been definitively identified. These currents may arise as the result of relatively small-scale fluctuations in buoyancy and wind forcing at the ocean surface. Alternatively, they may arise from various flow instability mechanisms such as baroclinic or barotropic instability. Tidal forcing and its interaction with topography is yet another possibility. In the present modeling situation of an idealized doubly periodic box, we are imposing random fluctuations in the near-surface ocean flow field as a surrogate for the real fluctuations that arise naturally from the kind of physical processes just mentioned. The goal of this paper is to focus on the response of the sea ice to the presence of turbulent, geostrophic eddies in the near-surface ocean currents and not on the exact physical mechanisms that lead to the presence of such eddy fields in the first place.

In the coupled model, a single layer of sea ice floats atop the ocean mixed layer. At model start, the sea ice is set to have a mean thickness of $\overline{h}_i = 1.00$ m and mean concentration of $\overline{C}_i = 95\%$. This is an idealization of the observed polar winter ocean–sea-ice field (Gloersen et al. 1992), and is more so relevant to the Antarctic pack than the thicker and more highly concentrated Arctic. On the horizontal scale of the entire model domain, that is, 100 km, it is to be expected that there is a naturally occurring SGS variation in both the sea-ice thickness and concentration fields. Such variations, particularly with respect to concentration, are not captured in a coarse-resolution model that treats the entire 100-km grid of the present study as equivalent to a single grid cell having homogeneous sea-ice properties. As an estimate of the kinds of variations that could typically occur on a fine-resolution domain, in this study we randomly distribute the sea-ice thickness between the values of 0 and $2\overline{h}_i$ using a uniform probability distribution. This distribution maintains the mean sea-ice thickness at the $\overline{h}_i = 1.00$ m value. Similarly, it is to be expected that there occur variations in the sea-ice concentration field that allows fluctuations from the mean value of $\overline{C}_i = 95\%$. As the sea-ice concentration has a physical upper bound of 100%, we choose to randomly distribute the sea-ice concentration between the values of 90% and 100%, again using a uniform probability distribution. This distribution maintains the mean concentration at the $\overline{C}_i = 95\%$ value. The initial states of the sea-ice thickness and concentration fields are shown in Fig. 2.

We have stated that the span of our entire fine-resolution numerical grid, which contains slightly more than 10 000 grid points, represents a spatial area that is typically covered by a single grid cell of a coarse-resolution climate model. In a fine-resolution model, if there are no SGS fluctuations in the ocean currents, either simply because there is no ocean current or if present it is horizontally uniform, then the sea-ice thickness and concentration fields will not evolve away from their initially assigned mean values. In such an unrealistic setting, where there exists no finescale fluctuating ocean currents, there is no meaningful distinction to be made between a coarse-resolution model and a fine-resolution one. That is, both the coarse-resolution and fine-resolution will produce time invariant mean sea-ice thickness and concentration fields, at least when there is no thermodynamical forcing. The absence of such thermodynamics is justified in the present context as we are attempting to elucidate but a single facet of the dynamical interaction between sea ice and ocean. Thermodynamics, while obviously important to sea-ice evolution, would only serve to obfuscate the dynamical effect presently targeted.

If the evolution of sea-ice characteristics is to be notably different between a single grid cell of a coarse-resolution climate model and the equivalent, many grid cells of a fine-resolution model, such as in the present study, then a possible explanation for that difference may reside with the fact that a fine-resolution model can explicitly resolve the ocean eddy field. It is singularly that aspect of the complex sea-ice–ocean system that we are studying presently. The underlying implication being that a fine-resolution model may have a very different sea-ice–ocean stress interaction than a coarse-resolution one. However, the ability to resolve the ocean eddy field would be, in itself, of no consequence if all that it served to do was to transport sea ice from one fine-resolution grid cell to another and so on. In that type of scenario the mean sea-ice thickness and concentration, averaged over the equivalent area of a single cell of a climate model, would not be affected. It is only when a well-resolved ocean eddy field leads to a nonlinear interaction between sea ice located in neighboring (fine resolution) grid cells that an impact can at all be felt. Such a nonlinear interaction is indeed potentially present in the model sea-ice–ocean system in so far as the parameterization of sea ice as a plastic fluid means that the sea ice responds fundamentally differently to convergent than to divergent strains. If during convergent motion sea ice does not undergo any plastic failure on the fine-resolution grid then nonlinearity effects are not present and the mean sea-ice statistics on the fine-resolution grid will be the same at those on the coarse-resolution grid. Interestingly, if sea ice does un-

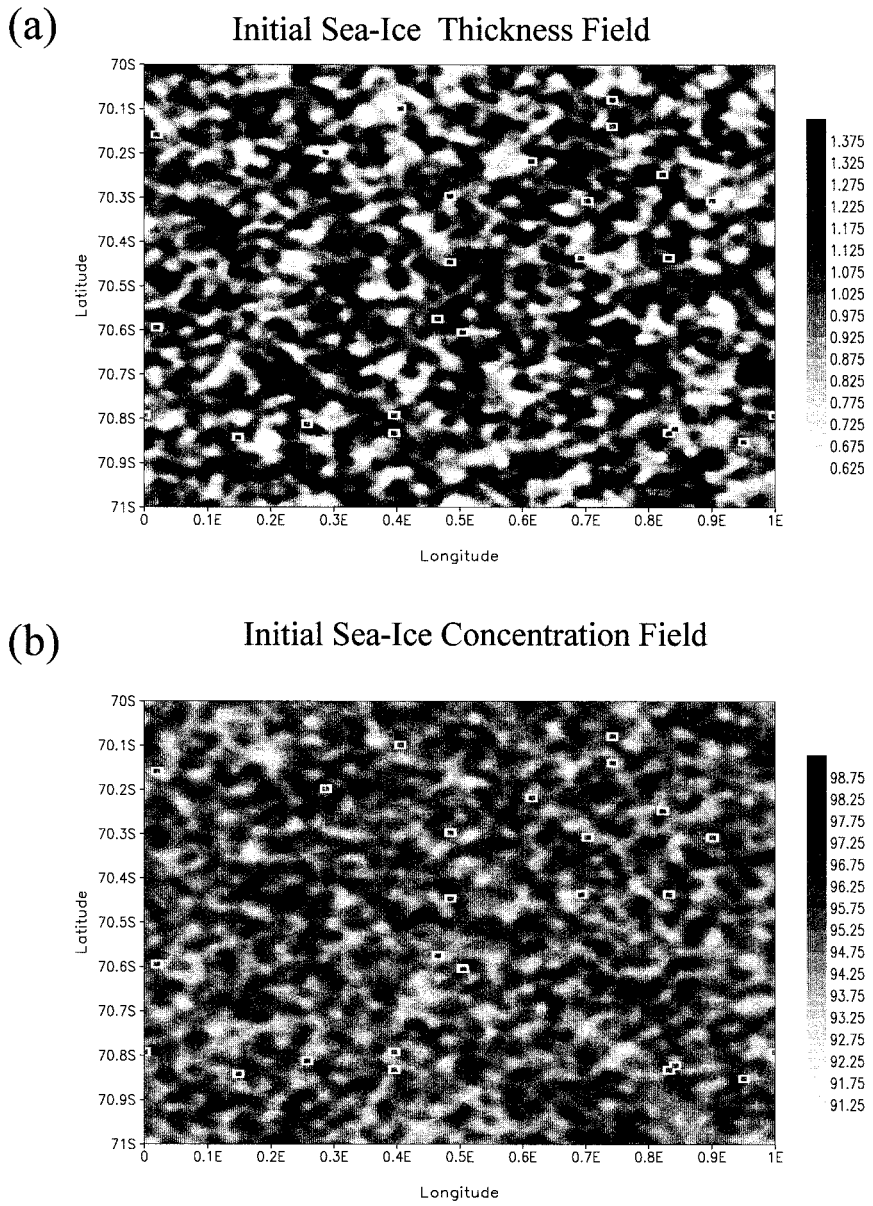

FIG. 2. Initial conditions for the sea-ice model fields. (a) The sea-ice thickness, of mean value $\overline{h}_i = 1.00$ m, is randomly distributed over the model domain grid points following a uniform probability distribution of $\overline{h}_i \pm 1.00$ m. The small, embedded rectangles represent grid cells that have effectively zero sea-ice thickness and are thus considered sea-ice free. The presence, at model initialization, of a few such sea-ice-free grid cells is consistent with the imposed uniform probability distribution on thickness. (b) The sea-ice concentration, of mean value $\overline{C}_i = 95.00\%$, is also randomly distributed but following a uniform probability distribution of $\overline{C}_i \pm 5.00\%$.

dergo plastic failure during convergent motion then an irreversible process is at work, that is, once sea-ice areal coverage is lost by convergence involving plastic failure that lost area fraction can not be recovered by any further dynamical process. It is this physical process, having an asymmetrical character in that it can potentially reduce sea-ice areal coverage but can not regenerate any increase in areal coverage, that we wish to highlight with our fine-resolution, ocean eddy-resolving numerical simulation. Such an irreversible process, if continually present, will serve to constantly reduce the net areal coverage of sea ice in a fine-resolution model. By comparison, a coarse-resolution model will hold its mean sea-ice concentration at a constant value as it has no inherent awareness of the stresses induced by the ocean eddy field, that it anyway fails to resolve.

We now complete the description of the details of the experimental configuration. The initial velocity field of

the sea ice, like that of the ocean, is motionless. During the model integration the sea ice moves due to the interfacial stresses that arise from the ocean eddy flow field. While random perturbations to the ocean surface currents are made throughout the model integration, no such random perturbations are imposed directly upon the sea-ice flow field.

The coupled model is integrated forward in time for an 11-day period. The relatively fine resolution of the model grid necessitates taking small time steps as noted earlier. Longer integration times are possible, though computationally expensive. The essential features of the sea-ice–ocean interaction that are to be illuminated in this study become apparent even after such a relatively short integration time, as is demonstrated in the results that follow.

b. Simulation results

By constantly seeding the ocean mixed layer currents with small, random perturbation velocities one can observe the development of a mixed layer velocity field that is relatively geostrophic and turbulent. In the absence of a background planetary rotation such a field would be turbulent due to the random nature of the input perturbation, but of course would not be geostrophic. However, as we indeed have a large background planetary vorticity field, the appearance of turbulent geostrophic eddies, having a length scale appropriate to that of the local baroclinic radius of deformation ($\sim$10 km), is quite evident in the mixed layer velocity field (Fig. 3).

In this study, the mixed layer velocity field provides the mechanical forcing that drives the evolution of the sea-ice field. The ocean velocity field contains both divergent and vortical strain components (Fig. 4). As mentioned earlier, it is the production of areas of sea-ice convergence that is of greatest interest since that is where plastic failure can occur, and thus can effectively lead to a sink of sea-ice concentration. A useful question to ask is: how is sea-ice convergence produced? The fact that the frictional planetary boundary layer, within which both the sea-ice and the ocean mixed layer reside, is highly rotational means that Ekman effects are present and that creation of convergent motion in the sea-ice cover is the result of both convergent strain and anticyclonic vorticity being present in the near-surface ocean current field. Distinct regions of ocean flow convergence (white areas in Fig. 4a) and of anticyclonic vorticity (black area in Fig. 4b) are indeed clearly present in the near-surface ocean current field. With respect to a coarse-resolution model grid, these strain-rate fields have a SGS variation pattern that is distributed randomly over the fine-resolution model grid.

Under the action of frictional stress, arising from the convergent and anticyclonic strain rates of the ocean surface velocity fields, some convergent sea-ice motion is in fact produced and the sea-ice cover evolves into a state at the end of the model integration (Fig. 5) that is quite different from its initial state (refer back to Fig. 2). Both the sea-ice thickness and concentration fields show that by the end of the simulation a few relatively large coherent, eddylike structures have appeared. The emergence of such structures is consistent, of course, with the presence of geostrophic eddies in the near-surface ocean currents as mentioned earlier (refer back to Fig. 3a). Not evident from the sea-ice thickness and concentration fields is the fact that although the thickness field has considerably rearranged itself from its initial randomly distributed spatial configuration, it still holds, on a domain-averaged sense, exactly the same mean thickness value as at model initialization, namely $\overline{h}_i = 1.00$ m. Interestingly though, the sea-ice concentration field, while also considerably rearranged from its initial state, has lost approximately 1% of its initial mean value of $\overline{C}_i = 95\%$.

To see why this might be so, we suspect it is likely that plastic failure has occurred and so produced this effect. The sea-ice pressure field (Fig. 6) shows that, as expected, there is significant variation in pressure over the model domain. The pressure field by itself is not very informative as it does not tell us where, if at all, plastic failure has occurred. This is because such failure is a function of not only the sea-ice pressure but also the maximum pressure tolerable by the particular sea-ice thickness and concentration that occurs in a given grid cell. For a given grid cell all of these quantities are constantly evolving and thus the locations where plastic failure can occur are constantly shifting throughout the model domain in response to variations in the turbulent, near-surface ocean flow field. We plot the ratio of the local sea-ice pressure to the local plastic failure strength (Fig. 6b) and see that failure occurs sporadically throughout the domain (intense black shading). The few grid points where plastic failure occurs represent a small but important sink on the sea-ice concentration field that has no counterpart in a coarse-resolution sea-ice–ocean model simulation.

The distinction in the evolution of the mean sea-ice thickness $\overline{h}_i$, which remains essentially constant, as compared to that of the sea-ice concentration $\overline{C}_i$, which drops by almost 1%, is made more evident by plotting time series of these two quantities for the entire model integration period (Fig. 7).

4. Conclusions

We now briefly review the main points and research findings of this paper. A coupled sea-ice–ocean model has been presented. The ocean model is an existing isopycnic ocean model (i.e., MICOM; Bleck et al. 1992), while the sea ice has been formulated by exactly mimicking the physics and numerics framework of a generic isopycnic layer of the ocean model and converting it into a sea-ice layer. In converting an isopycnic layer to a sea-ice layer attention was paid so that the Newtonian

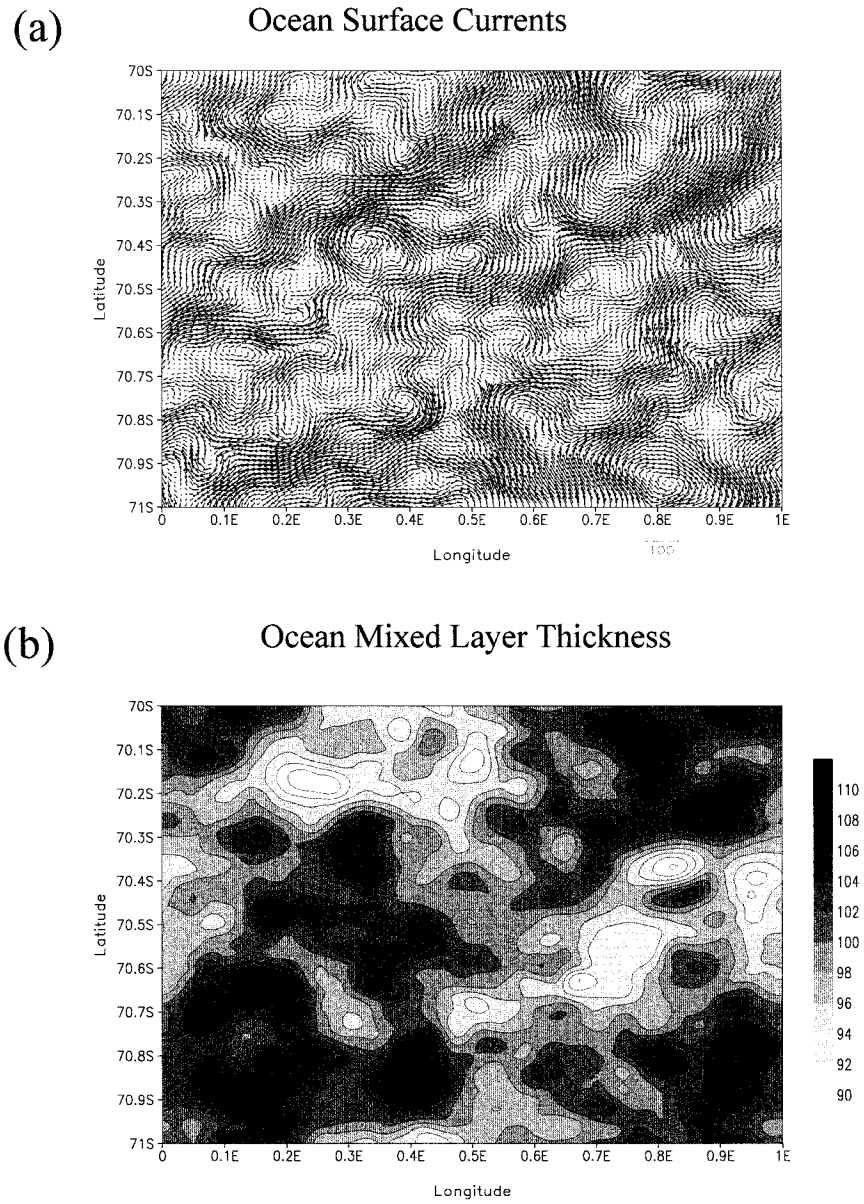

FIG. 3. State of the ocean mixed layer (a) currents (cm s^{-1}) and (b) thickness (m) at the end of the model simulation. Evident is the appearance of relatively coherent structures having an eddylike shape. The typical velocity is of order 30 cm s^{-1} and the typical perturbation to the initially horizontally homogeneous mixed layer is about 10 m. These eddy structures appear with approximately equal likelihood as being either cyclonic or anticyclonic.

formulation of viscosity for seawater was replaced with an appropriate cavitating-fluid rheology for sea ice (Flato and Hibler 1992). While the sea-ice and ocean model system is thus coupled both in a dynamical and a thermodynamical sense, the scope and focus of this study is on the implications of the dynamical coupling alone.

This study has been motivated by the observation that in nature the sea-ice field can apparently be influenced by the presence of geostrophic eddies occurring in the near-surface ocean currents. It is generally believed that oceanic flow instabilities are more pronounced in the near-coastal zone than in the open ocean, basically due to the presence of lateral boundaries and their associated frictional effects. Certainly, the swirling sea-ice fields of Fig. 1 occur in ocean waters adjacent to such a coastal zone. But instabilities can occur elsewhere, as for example, in the open ocean along strong density fronts. This study points out that actually resolving the ocean eddy field does have a measurable impact of the evolution of the modeled sea-ice fields, particularly the sea-ice concentration. The model simulation shows that the near-surface ocean eddy field acts to continually reduce

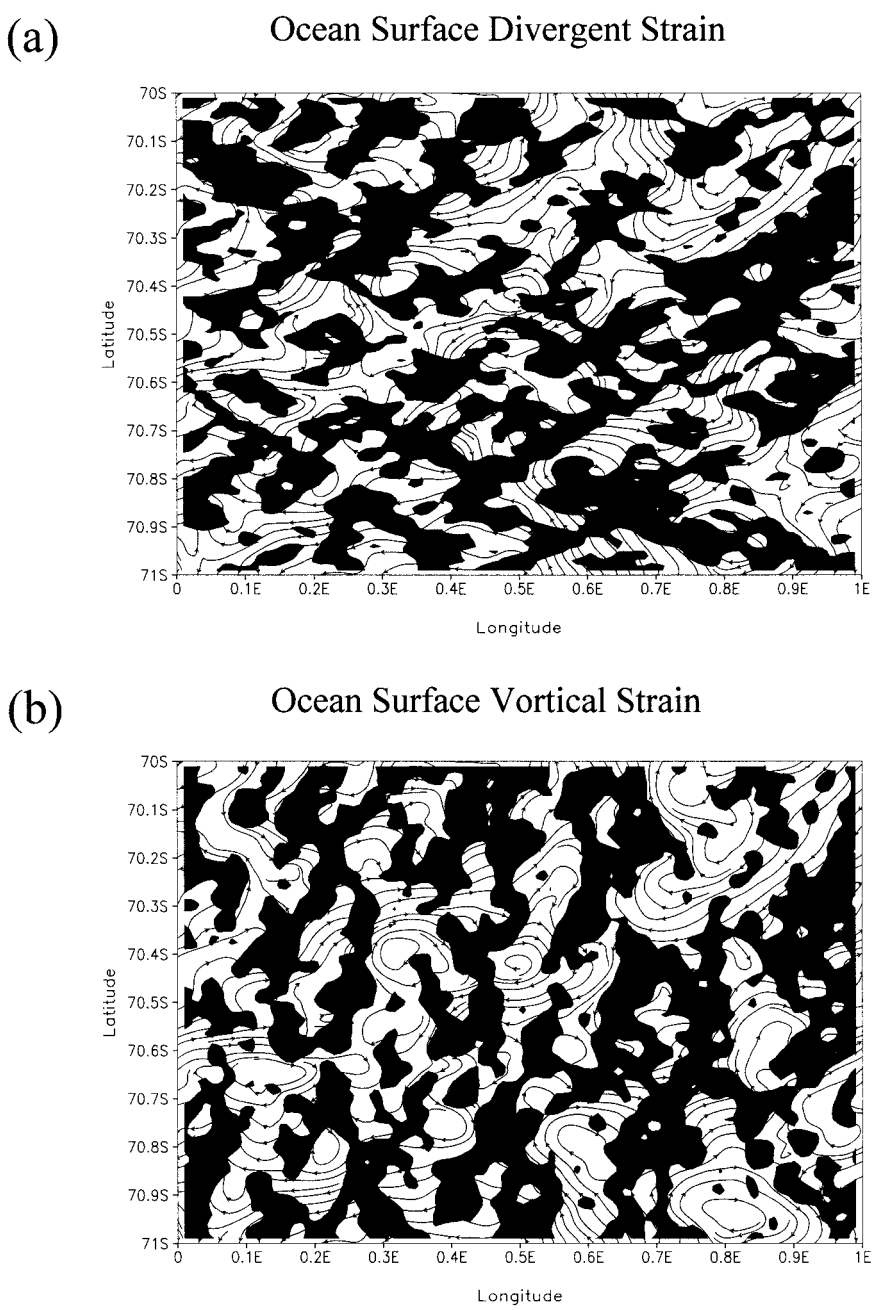

FIG. 4. Divergent and vortical strain-rate components of the ocean mixed layer flow field at the end of the simulation. (a) The divergent component of the strain field is shown with black shading representing area where the currents are undergoing divergent strain; the white areas represent convergent strain. For reference, the streamlines of the ocean mixed layer flow overlay the shading. (b) The vortical component of the strain field is shown with black shading representing anticyclonic vortical strain; the white areas represent cyclonic vortical strain.

the sea-ice concentration. This sink of sea-ice concentration will likely occur in coastal zones but also in any region where large enough near-surface ocean flow instabilities arise.

The physical mechanism responsible for the generation of this continual sink of sea-ice concentration is the plastic failure of the sea-ice cover. This can occur when, coincidentally, sufficiently strong strain rates in the near-surface ocean currents interact with a sufficiently thin sea-ice cover so as to cause a net convergence of the sea ice. Due to the random nature in which sea-ice floes move about and the turbulent nature of the near-surface ocean flows, there always exists some probability that such convergences can happen. In such sit-

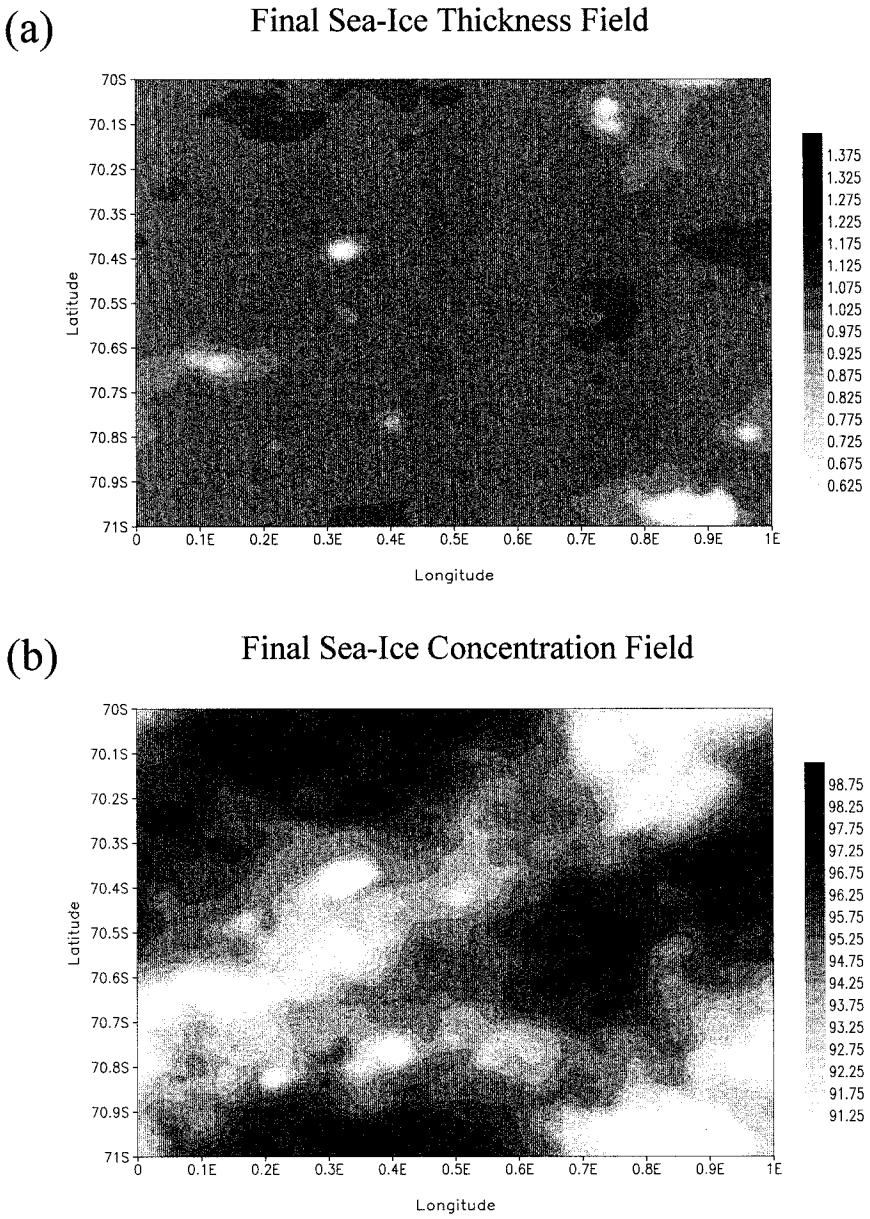

FIG. 5. State of the sea-ice model fields at the end of the simulation. (a) The sea-ice thickness (m) shows evidence pointing to the emergence of coherent structures. In particular, thin sea-ice areas, demarcated by the white areas, have appeared that were not present at model initialization. (b) The sea-ice concentration (%) also shows evidence of coherent structures. The white areas represent reduced sea-ice coverage that can reach values as low as 50%.

uations, the overall ice volume is precisely conserved but the mean sea-ice areal coverage is denigrated.

While this study has explored but one dynamical aspect of sea-ice–ocean interaction, it has nonetheless, implications for thermodynamic exchange between the ocean and atmosphere in the polar regions. Because a fine-resolution model will resolve the ocean eddy field and may therefore effectively have a continual sink of sea-ice concentration, such a model may realize a more efficient vertical transfer of heat and freshwater fluxes between the ocean and atmosphere. This being a direct consequence of the potential production of a greater lead fraction in the sea-ice cover of a fine-resolution model.

Intentionally, this study has been designed to investigate horizontal scales of motion that are smaller than a typical climate model grid scale. As a side effect of introducing random fluctuation into the ocean surface currents, inertial oscillations were also generated in the motion of the individual floes making up the fine-resolution grid sea-ice cover. At the latitude of the model

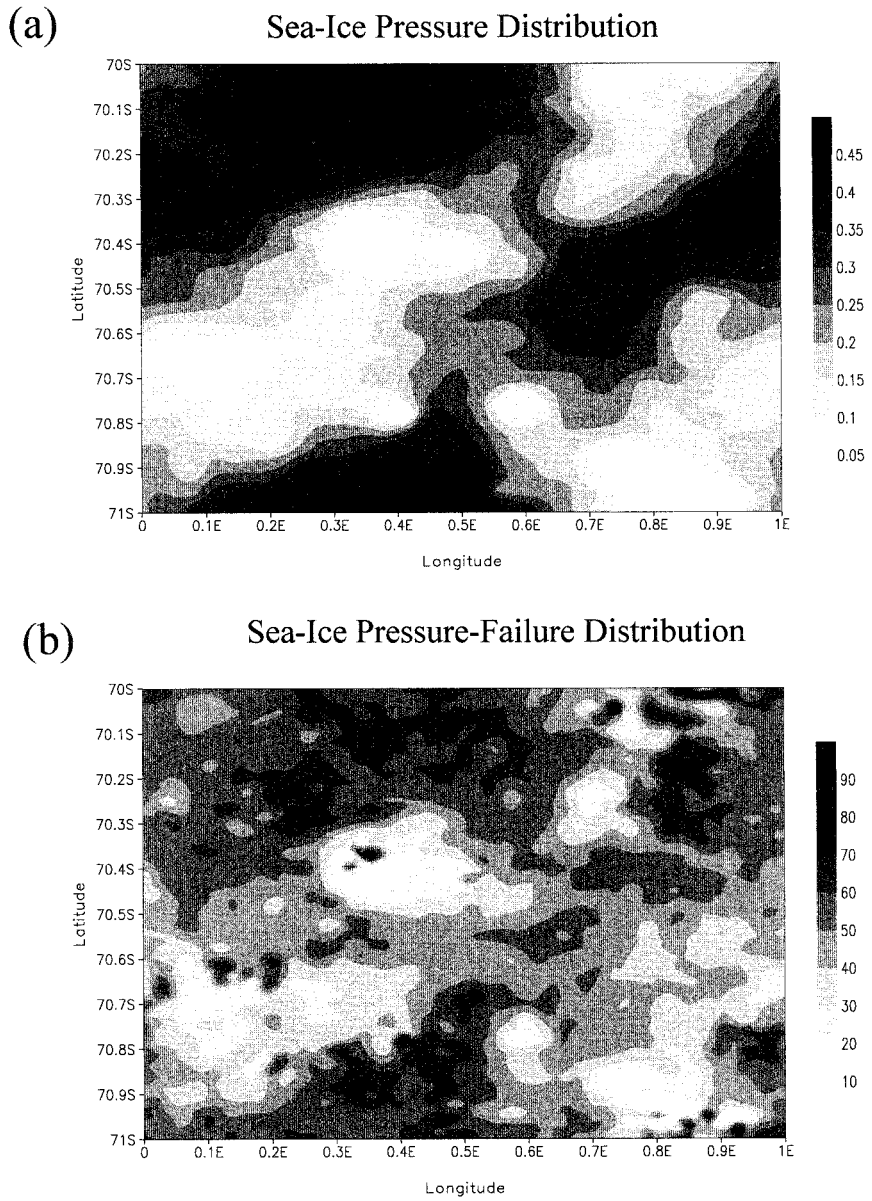

FIG. 6. State of the sea-ice pressure at the end of the simulation. (a) Sea-ice internal pressure field (kN m^{-1}) computed based on a quadratic-thickness strength formulation (Overland and Pease 1988) used in a cavitating fluid rheology scheme (Flato and Hibler 1992). (b) Ratio of local sea-ice internal pressure to the local, failure-limited pressure expressed as a percentage. Grid points in the model domain where the internal pressure exceeds that of the failure-limited pressure undergo a plastic failure. The intense black shading shows sporadic areas where such failure is occurring.

domain, these oscillations have a period of approximately 12 h and because neighboring ice floes are most likely to undergo individual inertial oscillations that are somewhat *out* of phase then these oscillations contribute to the overall SGS effects on the sea-ice cover in this study. In other words, the inertial oscillations are not likely to make all the sea-ice floes move in a coherent, large-scale and thus noninteracting fashion. Not modeled in this study were tidal oscillations, which coincidentally also have a component forced at an approximately 12-h period. They were not included because the tidal currents are generally of a coherent, horizontal scale much greater than that of a typical climate model grid cell and may therefore not contribute on the smaller scales of interest here. On the other hand, the possible interactions of the tidal flow with near-coastal topography could lead one to draw the opposite conclusion.

While the model experiment has utilized random fluctuations in the ocean currents to generate geostrophic turbulence in the ocean, it would be equally plausible

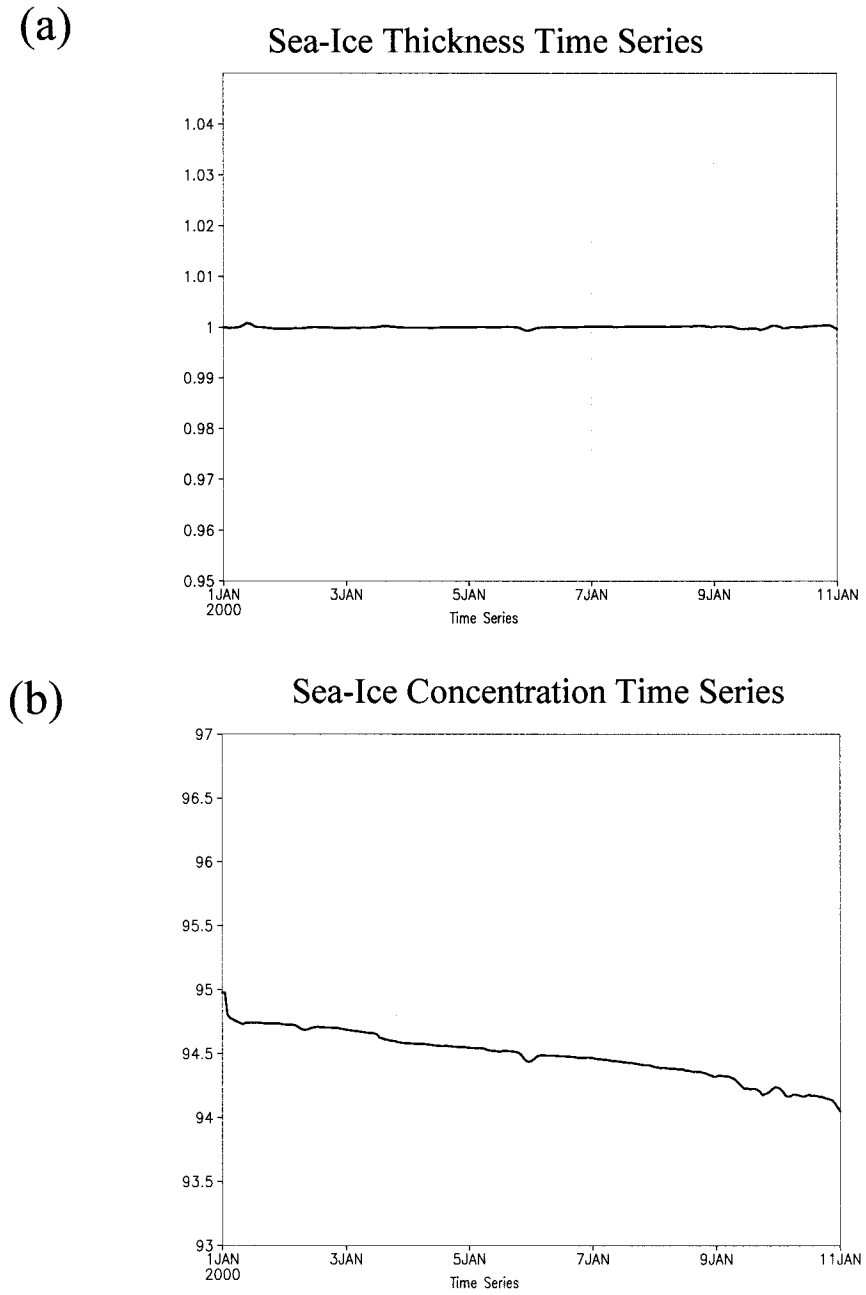

FIG. 7. Time series of evolution of the model sea-ice fields throughout the entire model integration. (a) The sea-ice thickness (m) holds very close to its initial, domain-averaged value of $\overline{h}_i = 1.00$ m. (b) The sea-ice concentration (%), however, shows a near-constant downward trend, effectively indicating a continual loss of sea-ice areal coverage. Note that the sea-ice thickness, as defined in this study, is the gridcell-averaged thickness.

to impose fluctuations in the mean atmospheric wind fields. While it is true that atmospheric eddies, that is, cyclones, tend to have a horizontal scale much larger than a typical climate model grid cell, there exists nonetheless, turbulent fluctuations in the wind field at a scale below that of a climate model grid cell that may indeed have impact on the evolution of the sea-ice cover. Atmospheric winds were not employed in the present study as we have been focusing on fluctuations in the ocean currents. Future studies will address the question of the role of fluctuations in the wind fields and that of the tidal currents, mentioned above.

In may be that in the future a suitable parameterization of the SGS process discussed in this paper will be developed, in which instance particular attention will need to be paid to the assumption of the sea ice as being

a continuum medium. When dealing with parameterizations of SGS phenomenon in a sea-ice context, one has to be more cautious than in the analogous atmospheric or oceanic contexts because of the fact that sea ice, while conventionally treated as a continuum down to the smallest possible scales, is ultimately not a continuum fluid but consists of floes of wildly varying shape and size. While large-scale sea-ice models, used as component models of coupled climate models, treat sea ice as a continuum fluid, one has to recognize that as the horizontal grid scales become finer and finer, as a result of improved computing power, there may quickly come a point at which one is forced to acknowledge that the sea-ice fields actually consists of a wide array of *individual* floes. The question naturally arises, at what horizontal scale, if any, does the continuum hypothesis currently underlying our sea-ice equations break down? By contrast, it is obvious that for atmospheric and oceanic SGS processes no such horizontal-scale limitations exist, that is, we can treat such fluids at continuous for all practical purposes. We need always keep this caveat in mind when contemplating developing SGS parameterizations of sea-ice-related processes.

It has often been noted that some of the most challenging issues remaining in sea-ice–ocean modeling are associated with parameterizing the effects of physical processes occurring on time- and space scales smaller than can be represented by climate models. The sea-ice and ocean component models of global climate models will continue, for the most part, to have relatively coarse spatial resolution. The idea of not at all resolving the effects of ocean eddies in climate simulations or, more to the point, doing so inaccurately is not acceptable practice and so there exists incentive to develop more skillful parameterization for marginally resolved eddy solutions (McWilliams 1998). The present study has served to highlight that the interaction of the sea-ice cover with the near-surface ocean eddy field is capable of producing extra lead area in fine-resolution simulations that is not concomitant to that produced in coarse-resolution simulations. Awareness of this issue will hopefully prompt some interest in the future development of a suitable, physically based parameterization that mimics this sea-ice–ocean interaction effect when relatively coarse-resolution model grids are employed in climate studies.

Acknowledgments. The satellite image of sea-ice cover (Fig. 1) was provided courtesy of Mark Drinkwater of the Jet Propulsion Laboratory, Pasadena, California, and the Canadian Space Agency, ADRO Project 164. Andy Majda is thanked for sponsoring a workshop at the Courant Institute of Mathematical Sciences (December, 1999) relating to the modeling of SGS phenomena in geophysical contexts. Discussions held at that workshop led to this paper. The author gratefully acknowledges support from the Office of Polar Programs of the National Science Foundation Grants OPP-9901039, OPP-9984966, and OPP-0084286 and from the Polar Research Program of the National Aeronautical Space Administration Grant NAG-5-8475. Supercomputing time was provided by the Arctic Region Supercomputing Center, University of Alaska, Fairbanks, Alaska.

REFERENCES

Arakawa, A., and V. R. Lamb, 1977: Computational design of the basic processes of the UCLA General Circulation Model. *Methods Comput. Phys.,* **17,** 174–265.

Asselin, R., 1972: Frequency filter for time integrations. *Mon. Wea. Rev.,* **100,** 487–490.

Bleck, R., 1998: Ocean modeling in isopycnic coordinates. *Ocean Modeling and Parameterization,* E. P. Chassignet and J. Verron, Eds., Kluwer Academic, 423–448.

——, and L. T. Smith, 1990: A wind-driven isopycnic coordinate model of the north and equatorial Atlantic Ocean. 1. Model development and supporting experiments. *J. Geophys. Res. (Oceans),* **95,** 3273–3285.

——, C. Rooth, D. M. Hu, and L. T. Smith, 1992: Salinity-driven thermocline transients in a wind-forced and themohaline forced isopycnic coordinate model of the North Atlantic. *J. Phys. Oceanogr.,* **22,** 1486–1505.

Brydon, D., S. Sun, and R. Bleck, 1999: A new approximation of the equation of state for seawater, suitable for numerical ocean models. *J. Geophys. Res. (Oceans),* **104,** 1537–1540.

Claussen, M., 1991: Estimation of areally-averaged surface fluxes. *Bound.-Layer Meteor.,* **54,** 387–410.

Climate Research Committee, 1995: *Natural Climate Variability On Decade-to-Century Time Scales.* National Academy Press, National Research Council, 630 pp.

Duffy, P. B., and K. G. Caldeira, 1999: Sensitivity of simulated salinities in a three dimensional ocean general circulation model to vertical mixing of destabilizing surface fluxes. *Climate Dyn.,* **15,** 81–88.

Fahrbach, E., G. Rohardt, M. Schröder, and V. Strass, 1994: Transport and Structure of the Weddell Gyre. *Ann. Geophys.,* **12,** 840–855.

Flato, G. M., and W. D. Hibler, 1992: Modeling pack ice as a cavitating fluid. *J. Phys. Oceanogr.,* **22,** 626–651.

Gaspar, P., 1988: Modeling the seasonal cycle of the upper ocean. *J. Phys. Oceanogr.,* **18,** 161–180.

Gent, P. R., and J. C. McWilliams, 1990: Isopycnal mixing in ocean circulation models. *J. Phys. Oceanogr.,* **20,** 150–155.

Gloersen, P., W. J. Campbell, D. J. Cavalieri, J. C. Comiso, C. L. Parkinson, and H. J. Zwally, 1992: *Arctic and Antarctic Sea Ice, 1978–1987: Satellite Passive-Microwave Observations and Analysis.* National Aeronautics and Space Administration, 290 pp.

Grotzner, A., R. Sausen, and M. Claussen, 1996: The impact of subgrid scale sea-ice inhomogeneities on the performance of the atmospheric general circulation model ECHAM3. *Climate Dyn.,* **12,** 477–496.

Hibler, W. D., 1979: A dynamic thermodynamic sea-ice model. *J. Phys. Oceanogr.,* **9,** 815–846.

——, 1980: Modeling a variable thickness sea ice cover. *Mon. Wea. Rev.,* **108,** 1943–1973.

Holland, D. M., 1998: On the parameterization of basal heat flux for sea-ice modeling. *Geophysica,* **34,** 1–21.

——, and A. Jenkins, 1999: Modeling thermodynamic ice–ocean interactions at the base of an ice shelf. *J. Phys. Oceanogr.,* **29,** 1787–1800.

——, L. A. Mysak, D. K. Manak, and J. M. Oberhuber, 1993: Sensitivity study of a dynamic thermodynamic sea ice model. *J. Geophys. Res. (Oceans),* **98,** 2561–2586.

McFarlane, N. A., 1987: The effect of orographically excited gravity-wave drag on the circulation of the lower stratosphere and troposphere. *J. Atmos. Sci.,* **44,** 1775–1800.

McWilliams, J. C., 1998: Oceanic general circulation models. *Ocean Modeling and Parameterization,* E. P. Chassignet and J. Verron, Eds., Kluwer Academic Publisher, 1–44.

Millero, F. J., C. T. Chen, A. Bradshaw, and K. Schleicher, 1980: A new high pressure equation of state for seawater. *Deep-Sea Res.*, **27,** 255–264.

Olbers, D. J., V. Gouretzki, G. Seiss, and J. Schroeter, 1992: *The Hydrographic Atlas of the Southern Ocean.* Alfred Wegener Institute, 82 pp. [Available online at http://www.awi-bremerhaven.de/Atlas/SO.]

Overland, J. E., and C. H. Pease, 1988: Modeling ice dynamics of coastal seas. *J. Geophys. Res.*, **93,** 15 619–15 637.

Rothrock, D. A., Y. Yu, and G. A. Maykut, 1999: Thinning of the Arctic sea-ice cover. *Geophys. Res. Lett.*, **26,** 3469–3472.

Smagorinsky, J. S., 1963: General circulation experiments with the primitive equations. I: The basic experiment. *Mon. Wea. Rev.*, **91,** 99–164.

Steele, M., and T. Boyd, 1998: Retreat of the cold halocline layer in the Arctic Ocean. *J. Geophys. Res.*, **103,** 10 419–10 435.

Stossel, A., and M. Claussen, 1993: On the momentum forcing of a large-scale sea-ice model. *Climate Dyn.*, **9,** 71–80.

Thompson, D. W. J., and J. M. Wallace, 1998: The Arctic Oscillation signature in the wintertime geopotential height and temperature fields. *Geophys. Res. Lett.*, **25,** 1297–1300.

Thorndike, A. S., D. A. Rothrock, G. A. Maykut, and R. Colony, 1975: The thickness distribution of sea ice. *J. Geophys. Res.*, **80,** 4501–4513.

White, W. B., and R. G. Peterson, 1996: An Antarctic circumpolar wave in surface pressure, wind, temperature and sea-ice extent. *Nature,* **380,** 699–702.